Anthropogenic forcing on tropospheric ozone and OH since preindustrial times

Yuhang Wang

School of Earth and Atmospheric Sciences, Georgia Institute of Technology, Atlanta

Daniel J. Jacob

Department of Earth and Planetary Sciences and Division of Engineering and Applied Sciences, Harvard University, Cambridge, Massachusetts

Abstract. A global three-dimensional model of tropospheric chemistry is used to investigate the changes in tropospheric O_3 and OH since preindustrial times as a result of fuel combustion and industry, biomass burning, and growth in atmospheric CH_4. Model results indicate a 63% increase of the global tropospheric O_3 burden from preindustrial times to present (80% and 50% in the northern and southern hemispheres, respectively). Anthropogenic emissions of NO_x and of CO and hydrocarbons make comparable contributions to the global O_3 increase (60% and 40% respectively), even though the local rate of tropospheric O_3 production is generally NO_x limited. The rise in O_3 production parallels closely the rise in the emissions of CO and hydrocarbon because the O_3 yield per mole of CO or hydrocarbon oxidized has remained constant at 0.7-0.8 mol/mol since preindustrial times. In contrast, the O_3 production efficiency per mole of NO_x emitted has decreased globally by a factor of 2. We find a 9% decrease in the global mean OH concentration (mass-weighted) since preindustrial times. A linear relationship is found in the model between the global mean OH concentration and the $S_N/S_C^{3/2}$ ratio, where S_N and S_C are the sources of NO_x and of CO and hydrocarbons, respectively. The relative constancy of the global mean OH concentration since preindustrial times reflects the conservation of the $S_N/S_C^{3/2}$ ratio despite large increases in both S_N and S_C. Comparisons of model results with reconstructed nineteenth century observations of O_3 at continental sites indicate a systematic overestimate of about 5 ppbv. Correcting this overestimate would require either a large missing chemical sink for O_3 or a downward revision of the natural NO_x source from lightning (3 Tg N yr^{-1} in our model). The nineteenth century observations of O_3 over France show no vertical gradient between the boundary layer and the free troposphere, which is inconsistent with our current understanding of tropospheric O_3. The model underestimates preindustrial CO concentrations derived from polar ice cores; these measurements are difficult to reconcile with any reasonable CO emission inventories.

1. Introduction

Preindustrial measurements of O_3 concentrations at surface sites in western Europe and South America indicate an increase of several fold from preindustrial times to present [*Volz and Kley*, 1988; *Anfossi et al.*, 1991; *Sandroni et al.*, 1992; *Marenco et al.*, 1994]. This increase is likely driven by anthropogenic emissions of NO_x ($NO+NO_2$), CO, and hydrocarbons from fossil fuel combustion and biomass burning. Increasing concentrations of O_3, NO_x, CO, and hydrocarbons may have also induced significant changes in the abundance of tropospheric OH, the main atmospheric oxidant [*Thompson*, 1992]. Since tropospheric O_3 is a greenhouse gas and OH concentrations determine the lifetimes of greenhouse gases such as CH_4 and hydrochlorofluorocarbons (HCFCs), anthropogenic perturbations to tropospheric O_3 and OH have important implications for climate change [*Intergovernmental Panel on Climate Change (IPCC)*, 1996].

A number of model studies have attempted to describe the changes of tropospheric O_3 and OH concentrations since preindustrial times: one-dimensional models before the early 1990s [*Thompson*, 1992] and two- and three-dimensional models more recently [*Crutzen and Zimmermann*, 1991; *Thompson et al.*, 1993; *Martinerie et al.*, 1995; *Lelieveld and Van Dorland*, 1995; *Kasibhatla et al.*, 1996; *Levy et al.*, 1997; *Roelofs et al.*, 1997; *Berntsen et al.*, 1997]. Three-dimensional model simulations suggest an increase in global O_3 concentrations since preindustrial times ranging from 40% [*Levy et al.*, 1997; *Roelofs et al.*, 1997] to 70% [*Lelieveld and Van Dorland*, 1995]. The estimated change of the global mean OH concentration ranges from a 20% decrease [*Thompson et al.*, 1993] to a 6-7% increase [*Martinerie et al.*, 1995; Berntsen et al., 1997]. The relatively small OH changes in these models reflect compensating anthropogenic influences from large increases in NO_x and O_3, which tend to enhance OH, and large increases in CO and hydrocarbons, which tend to deplete OH [*Thompson*, 1992].

We use in this work a global three-dimensional model of

tropospheric O_3-NO_x-hydrocarbon chemistry [*Wang et al.*, 1998a, b, c] to better understand how anthropogenic emissions have driven changes in O_3 and OH concentrations since preindustrial times. A brief description of the model is given in section 2, and results for the preindustrial and present atmospheres are presented in section 3. The model has been evaluated previously with observations for the present atmosphere [*Wang et al.*, 1998b], and we extend in section 4 this evaluation to reconstructed observations of O_3, CO, and OH proxies from the nineteenth century. In section 5, we interpret changes in O_3 and OH concentrations over the past century on the basis of changing anthropogenic emissions. Conclusions are in section 6.

2. Model Description

Our global three-dimensional model for tropospheric O_3-NO_x-hydrocarbon chemistry is described by *Wang et al.* [1998a]. The model is driven by meteorological fields archived every 4 hours from a general circulation model developed at the Goddard Institute for Space Studies [*Hansen et al.*, 1983]. It has a spatial resolution of 4° latitude by 5° longitude with seven vertical layers extending from the surface to 150 mbar. The model transports 15 chemical tracers: odd oxygen ($O_x = O_3 + O + NO_2 + HNO_4 + 2 \times NO_3 + 3 \times N_2O_5$), NO_x ($NO + NO_2 + NO_3 + HNO_2$), N_2O_5, HNO_3, HNO_4, peroxyacylnitrates, alkylnitrates, CO, ethane, ($\geq C_4$) alkanes, ($\geq C_3$) alkenes, isoprene, acetone, higher ketones, and H_2O_2. Spatially and seasonally varying flux boundary conditions are specified at 150 mbar to represent the cross-tropopause transport of O_3 (400 Tg O_3 yr^{-1}) and of total reactive nitrogen NO_y (0.48 Tg N yr^{-1}). The present-day simulation includes anthropogenic sources from fuel combustion and industry (22 Tg N yr^{-1} of NO_x, 520 Tg CO yr^{-1}, and 56 Tg C yr^{-1} of nonmethane hydrocarbons (NMHCs)), biomass burning (12 Tg N yr^{-1} of NO_x, 520 Tg CO yr^{-1}, and 51 Tg C yr^{-1} of NMHCs), and soil emission of NO_x associated with fertilizer usage (1.3 Tg N yr^{-1}). Natural emissions are from lightning (3.0 Tg N yr^{-1} of NO_x), soils (4.7 Tg N yr^{-1} of NO_x), and vegetation (600 Tg C yr^{-1} of isoprene and 15 Tg C yr^{-1} of acetone). Dry deposition is computed with a resistance-in-series scheme.

The model simulation for the present atmosphere has been evaluated extensively by *Wang et al.* [1998b] with long-term measurements of O_3 (surface sites and ozonesondes) and CO (surface sites) and with aircraft measurements of NO, peroxyacetylnitrate (PAN), HNO_3, C_2H_6, acetone, and H_2O_2 in different regions of the troposphere. The model reproduces observed monthly mean concentrations of O_3 generally to within 10 ppbv and captures the observed seasonal variations of O_3 to within 1 month. Ozone concentrations tend to be overestimated in the tropical marine boundary layer and underestimated in the upper troposphere of the southern tropics. Observed concentrations of NO and PAN are reproduced generally to within a factor of 2; HNO_3 concentrations tend to be overestimated, sometimes several fold. Concentrations of CO are reproduced to generally within 10 ppbv and concentrations of H_2O_2 are reproduced to within a factor of 2. The global mean OH concentration simulated in the model yields a lifetime of 5.1 years for CH_3CCl_3 below 200 mbar against oxidation by OH, in agreement with the estimate of 4.9±0.3 years derived from long-term observations of CH_3CCl_3 by *Prinn et al.* [1995].

We simulate the preindustrial atmosphere (circa 1850) by removing anthropogenic emissions from the present-day simulation (Table 1). Natural emissions (vegetation, soils, and lightning) and cross-tropopause fluxes of O_3 and NO_y are assumed to be the same as in the present atmosphere. We exclude emissions from fossil fuel combustion and industry; *Dignon and Hameed* [1989] estimated a global NO_x source from fossil fuel combustion of 0.4 Tg N yr^{-1} in 1860, as compared to 22 Tg N yr^{-1} in 1980. We also exclude soil NO_x emission from fertilizer use. The concentration of CH_4 is specified at 0.8 ppmv on the basis of ice core data, as compared to 1.7 ppmv for the present atmosphere [*IPCC*, 1996]. Changes since preindustrial times in land use, meteorology, aerosols, and stratospheric O_3 columns are not considered.

Historical trends in biomass burning are uncertain. The Greenland ice core record of ammonia does not show a systematic trend over the past 150 years [*Fuhrer et al.*, 1996] implying a relative constant fire activity at high northern latitudes. However, biomass burning takes place principally in the tropics. As will be discussed in section 4, nineteenth century observations of O_3 in South America [*Sandroni et al.*, 1992] imply a much weaker tropical biomass burning source than that of today. Following *Crutzen and Zimmermann* [1991], we assume in our standard simulation that preindustrial biomass burning emissions are 10% of the present-day value and retain the same geographic distribution. We also conduct a sensitivity simulation assuming a preindustrial biomass burning source the same as that of today.

Nitrate records in polar ice cores offer some indication of trends in combustion since preindustrial times, but caution is necessary in interpreting these records owing to possible HNO_3 evaporation from snow and firn [*Dibb et al.*, 1998]. The Greenland observations show a factor of 3 increase in nitrate deposition since preindustrial times [*Mayewski et al.*, 1990], while our model results for Greenland give a factor of 6 increase. The Antarctic observations show large interannual variability in nitrate over the past century but no systematic trend [*Mayewski and Legrand*, 1990]. Our model indicates an increase of 50% in nitrate deposition over Antarctica owing to long-range transport of biomass burning emissions; such a trend could have been masked in the observations by the high interannual variability.

3. Ozone and OH: Preindustrial Versus Present Atmosphere

Simulated mean concentrations of O_3 and CO near the surface in July are shown in Figure 1 for the preindustrial and present atmospheres. Preindustrial O_3 concentrations in the northern hemisphere are about 10-15 ppbv and are lower than in the southern hemisphere (15-20 ppbv)

because of the larger amount of O_3 transported from the stratosphere in the winter hemisphere and the enhanced chemical loss of O_3 in the summer hemisphere. In contrast, present-day O_3 concentrations in the northern hemisphere (20-50 ppbv) are a factor of 2 to 4 higher than in preindustrial times and are also higher than in the present southern hemisphere (20-40 ppbv) owing to enhanced summertime photochemical production associated with emissions from fuel combustion and industry. Simulated CO concentrations are a factor of 2 to 5 lower in preindustrial times than at present owing to lower preindustrial concentrations of CH_4 and lower direct emissions of CO. Higher CO concentrations over the continents of the northern hemisphere in preindustrial times are due to CO production from the oxidation of isoprene.

Zonally averaged annual mean concentrations of O_3, OH, NO_x, and CO simulated for preindustrial and present atmospheres are shown in Figure 2a; relative changes from preindustrial times to present are shown in Figure 2b. Simulated O_3 concentrations for the preindustrial atmosphere show a much smaller interhemispheric asymmetry than at present. Somewhat higher O_3 concentrations in the northern than in the southern hemisphere in preindustrial times are due mostly to a larger stratospheric source in the northern hemisphere and a larger source of NO_x from soils. Model results indicate that mean tropospheric O_3 concentrations have increased since preindustrial times by 80% in the northern hemisphere and by 50% in the southern hemisphere. Concentrations in the upper troposphere, where O_3 is an effective greenhouse gas, have increased by 20-80%. This increase is largest in the tropics where O_3 transport from the stratosphere is negligible [*Holton et al.*, 1995].

We find that the global tropospheric O_3 burden (integrated from the surface up to 150 mbar) has increased by 63% from 4.0 x 10^{12} mol in preindustrial times to 6.5 x 10^{12} mol today. This increase is similar to the estimate of 70% by *Lelieveld and Van Dorland* [1995], but is higher than the estimates of 40% by *Levy et al.* [1997] and *Roelofs et al.* [1997]. The lower estimate by *Levy et al.* [1997] is likely due to their assumption of present-day CH_4 and CO concentrations for the preindustrial atmosphere; in our preindustrial simulation, increasing the concentration of CH_4 from 0.8 to 1.7 ppmv alone increases the global O_3 burden by 13%. The lower estimate by *Roelofs et al.* [1997] is due in part to a 40% decrease in the cross-tropopause O_3 flux from preindustrial times to present in their simulation. Some difference among the models is also expected from adoption of different tropopause levels for budget analysis.

Table 2 shows our global budgets of tropospheric O_3 for the preindustrial and present-day simulations. Our budget for the present atmosphere is discussed by *Wang et al.* [1998b, c] and is consistent with results from other recent three-dimensional models. Our estimate for chemical production of O_3 in the preindustrial troposphere is almost identical to the estimates by *Crutzen* [1994] and *Roelofs et al.* [1997], while our estimate for chemical loss of O_3 is 10% higher than *Crutzen* [1994] and 14% lower than *Roelofs et al.* [1997]. The lower estimate of chemical loss by *Crutzen* [1994] is due to a 40% higher O_3 loss to dry deposition than in our model; the higher estimate by *Roelofs et al.* [1997] is due to a 30% lower loss to dry deposition and a 50% higher cross-tropopause flux than in our model.

We find that the budget of tropospheric O_3 is dominated by chemical production and loss within the troposphere for both the present and preindustrial atmospheres. The globally averaged lifetime of O_3 has decreased by 20% since preindustrial times because most of the increase of O_3 concentrations has been in the lower troposphere (Figure 2b) where the lifetime of O_3 is shorter than in the middle and upper troposphere [*Wang et al.*, 1998c]. As a result, although chemical production of O_3 at present is more than twice that in preindustrial times, the O_3 burden in the troposphere is only 63% higher.

Our model results for OH indicate that concentrations have either increased or decreased since preindustrial times depending on the region (Figure 2b). This variability reflects largely the regional variability in the enhancements of NO_x and O_3, which tend to increase OH. Enhancements of CO and CH_4, which tend to decrease OH, are much more uniform in the troposphere. In the lower troposphere of the northern hemisphere, where NO_x and O_3 are strongly enhanced, OH concentrations show a 20-60% increase. In the middle and upper troposphere where NO_x and O_3 enhancements are modest, OH concentrations show a 20% decrease.

Preindustrial OH concentrations are almost symmetric across the equator, while present-day OH concentrations are higher in the northern than in the southern hemisphere. The impact of anthropogenic emissions on OH concentrations is asymmetric because the lifetimes of CO (a few months) and CH_4 (about 10 years) are much longer than that of NO_x (hours to days) allowing CO and CH_4 but not NO_x to be transported to the southern hemisphere from the northern hemisphere where 90% of the fossil fuel combustion source and most of CH_4 sources are located. The interhemispheric asymmetry in the change of OH concentrations was previously simulated by *Crutzen and Zimmermann* [1991]; the increase of OH concentrations in the lower troposphere of the northern hemisphere is larger and broader in our model than in theirs.

We find that the mass-weighted global mean OH concentration below 150 mbar has decreased by 9% from 1.15 x 10^6 molecules cm^{-3} (preindustrial) to 1.04 x 10^6 molecules cm^{-3} (present). However, the lifetime of CH_3CCl_3 against OH oxidation has remained at 5.1 years; the increase of OH concentrations in the lower troposphere, where the rate constant for CH_3CCl_3 oxidation is higher owing to warmer temperatures, has compensated for a lower present-day global mean OH concentration. Previous model calculations of the trend in the mass-weighted global mean OH concentration from preindustrial times to present indicated a 6-7% increase [*Martinerie et al.*, 1995; *Berntsen et al.*, 1997], a 3% decrease [*Lelieveld and Van Dorland*, 1995], a 10-15% decrease [*Crutzen and Zimmermann*, 1991], and a 22% decrease [*Roelofs et al.*, 1997]. Earlier estimates based largely on one-dimensional models indicated a 10-30% decrease [*Thompson*, 1992].

The general consensus among the current generation of models is that the global mean OH concentration has remained to within 20% of the present-day value since preindustrial times.

4. Model Evaluation With Preindustrial Observations

4.1. Ozone

Nineteenth century concentrations of O_3 at a number of continental sites have been reconstructed from old measurements made with impregnated papers and a colorimetric scale. A detailed review is given by *Marenco et al.* [1994]. According to this review, some early reconstructions including by *Linvill et al.* [1980] (15-50 ppbv in Michigan), *Bojkov* [1986] (15-26 ppbv at sites in North America and Europe), and *Lissac and Grubisich* [1991] (30-36 ppbv in Yugoslavia) have positive biases due to incorrect calibrations. For comparison with our model results, we use the reconstructed data by *Anfossi et al.* [1991] and *Marenco et al.* [1994] for France and Italy and those by *Sandroni et al.* [1991] for Argentina and Uruguay. These reconstructions used similar calibrations [*Marenco et al.*, 1994].

Figure 3 compares the reconstructed observations with model simulations of surface O_3 concentrations for the preindustrial atmosphere. The reconstructed data generally show O_3 concentrations of 7-12 ppbv. The weak winter-spring maximum in the European observations is reproduced by the model, where it reflects the stratospheric influence (Figure 3). Observations from South America show no significant springtime enhancement from biomass burning, in contrast to the present atmosphere [*Kirchhoff and Rasmussen*, 1990], implying a much weaker biomass burning source in preindustrial times than that of today. Including the present-day biomass burning source in our standard preindustrial simulation leads to a 10-20 ppbv increase of O_3 concentrations in northern Argentina and Uruguay during the austral burning season of August-November (Figure 3).

Figure 3 shows that our standard preindustrial simulation overestimates the reconstructed observations consistently by 0-20 ppbv. The discrepancies are particularly large in the winter season of both hemispheres, reflecting a greater seasonal amplitude in the model (driven by the stratospheric influence). The preindustrial observations in Figure 3 were typically taken around the clock, and some of the model overestimate may be due to nighttime O_3 depletion by dry deposition in a shallow stable surface layer sampled by the observations but not resolved by the model [*Jacob et al.*, 1993]. Negative interference to O_3 measurements by NH_3 or SO_2 could also contribute [*Anfossi and Sandroni*, 1997]. Loss of O_3 to natural organic aerosols or to a denser preindustrial vegetation canopy could further mitigate some of the overestimates in summer. These effects are, however, unlikely to explain the seasonal pattern of the overestimates and should not be an issue at Pic du Midi, a mountain site [*Marenco et al.*, 1994]. Model results from a sensitivity simulation in which O_3 transport from the stratosphere is excluded are in much better agreement with the reconstructed observations (Figure 3). However, there is no physical basis to suspect that O_3 transport from the stratosphere to the troposphere in preindustrial times was much less or had a different seasonal variation from present [*Holton et al.*, 1995].

Previous global three-dimensional model simulations of the preindustrial atmosphere show similar tendencies to overestimate observations. *Roelofs et al.* [1997] find mean surface O_3 concentrations over Europe of 10-15 ppbv in summer and 15-20 ppbv in winter, in good agreement with ours, while *Levy et al.* [1997] find corresponding values of 7-9 ppbv in summer and 20 ppbv in winter (H. Levy II., personal communication, 1997). The best simulation would appear to be that of *Berntsen et al.* [1997] which yields surface O_3 concentrations of 10 ppbv at Paris with little seasonal variation. However, that simulation assumes excessive O_3 deposition velocities: 0.5 cm s^{-1} in summer and 0.4 cm s^{-1} in winter over Europe referenced to 200 m altitude (lowest model layer) [*Berntsen and Isaksen*, 1997]. These values are about a factor of 2 too high when compared to resistance-in-series models which account for the effect of nighttime stability in the 0-200 m column and a lack of stomatal uptake of O_3 in winter [*Jacob et al.*, 1993; *Ganzeveld and Lelieveld*, 1995; *Munger et al.*, 1998; *Wang et al.*, 1998a].

The most troubling discrepancy in Figure 3 is at Pic du Midi (2.4 km altitude), where the preindustrial data should not be affected by chemical interferences from NH_3 or SO_2 and where local surface effects should be minimal [*Marenco et al.*, 1994]. Matching the nineteenth century Pic du Midi observations in our model, assuming the same stratospheric source as that of today and some natural NO_x emissions (lightning and soils), would require a large missing chemical sink of O_3 in the troposphere. A perplexing aspect of the Pic du Midi preindustrial observations is the lack of vertical gradient relative to Montsouris (Figure 3). Present-day vertical profiles of O_3 concentrations at remote continental sites typically show differences of 10-20 ppbv between the sea level and 2-3 km altitude as a result of chemical loss and dry deposition in the boundary layer [*Anderson et al.*, 1994; *Mauzerall et al.*, 1996]. *Anfossi et al.* [1991] found in the nineteenth century Moncalieri data that O_3 concentrations associated with downslope winds from the Alps (foehn) were 5-10 ppbv higher than average, suggesting an increase of O_3 concentrations with altitude which is at odds with the Pic du Midi data.

4.2. Carbon Monoxide

A recent analysis of ice core CO records shows concentrations of 91 ppbv in central Greenland for the period of 1802-1862 and 57 ppbv in Antarctica for the period of 1860-1916 [*Haan et al.*, 1996]. Figure 4 compares these data with model results for Greenland and Antarctica. The standard model for the preindustrial atmosphere is too low by a factor of 4 and does not show the observed interhemispheric asymmetry. When the present-day biomass burning

source is included, model results are still a factor of 2 too low and exhibit little interhemispheric asymmetry. As discussed in section 4.1, the reconstructed O_3 observations in South America imply a biomass burning source in the nineteenth century much less than that of today.

Previous model simulations for the preindustrial atmosphere, reviewed by *Haan et al.* [1996], also underestimate the ice core data. *Haan et al.* [1996] suggested that the underestimate could reflect the neglect of nineteenth century industrial emissions in the models. However, these emissions would have to be unrealistically large. As *Haan et al.* [1996] noted, the ice core record for 1860-1916 over Antarctica indicates CO concentrations similar to those observed today. The background CO concentration from CH_4 oxidation, however, has increased by 15 to 20 ppbv since preindustrial times. The ice core data for 1802-1862 over Greenland are not much lower than an annual mean concentration of 115 ppbv simulated in our model for the present atmosphere. The ice core data of *Haan et al.* [1996] would thus imply higher CO and NMHC emissions in the nineteenth century than at present in the southern hemisphere and comparable emissions in the northern hemisphere. Such a scenario is inconsistent with historical trends in fossil fuel combustion and is also inconsistent with the observed increase in tropospheric CO over Jungfraujoch (Switzerland) from 1950 to present [*Zander et al.*, 1989]. The Jungfraujoch measurements for 1950-1951 indicate 67 ppbv CO, which is lower than the Greenland ice core concentration of 91 ppbv reported by *Haan et al.* [1996] for the nineteenth century.

4.3. Hydrogen Oxide Radicals

Trends in the concentrations of hydrogen oxide radicals (HO_x=OH+HO_2) since preindustrial times have been estimated by *Staffelbach et al.* [1991] and *Anklin and Bales* [1997] using CH_2O and H_2O_2 records from Greenland ice cores. Interpretation of these records is subject to caution because of possible post-depositional exchange with the atmosphere, reactions within the ice, and secular changes in the seasonal accumulation of snow [*Neftel et al.*, 1995]. The record of CH_2O suggests a 30% decrease in OH concentrations since preindustrial times [*Staffelbach et al.*, 1991]; our corresponding model results over Greenland show a 12% decrease. Data for H_2O_2 in Greenland ice cores show constant concentrations from preindustrial times until about 1970 and a doubling of concentrations since then which would suggest a rise in HO_x concentrations [*Sigg and Neftel*, 1991; *Anklin and Bales*, 1997]. Our model shows a factor of 2.5 increase of H_2O_2 concentrations over Greenland from preindustrial times to today because of the increasing source of HO_x radicals as tropospheric O_3 concentrations increase.

5. Ozone and OH: Relationship to Anthropogenic Emissions

The major forcings of O_3 and OH concentrations since preindustrial times in our model are (1) the increase of CH_4 concentrations from 0.8 to 1.7 ppmv, (2) emissions of CO, NMHCs, and NO_x from fuel combustion and industry, and (3) emissions from biomass burning. We conducted three sensitivity simulations in which each forcing was individually added to the standard preindustrial simulation. We also conducted two additional sensitivity simulations in which the changes in emissions from preindustrial times to today were applied to either CO and NMHCs or to NO_x. The global mean OH concentrations for these simulations are shown in Table 1, and global budgets of tropospheric O_3 are shown in Table 2.

As discussed in section 3, OH concentrations reflect a balance between sources of CO and hydrocarbons (S_C) which deplete OH and sources of NO_x (S_N) which enhance OH. Table 1 shows values of S_C and S_N for our different simulations. In an analytical solution to a simple box model, we find that OH concentrations vary as $S_N/S_C^{3/2}$ (appendix). Our global three-dimensional model indeed exhibits a linear dependence of the global mean OH concentration on the $S_N/S_C^{3/2}$ ratio for the range of simulations conducted (Figure 5), but the large intercept of the linear regression line implies a much smaller OH sensitivity to $S_N/S_C^{3/2}$ than implied by the box model analysis. This dampening of the OH sensitivity to $S_N/S_C^{3/2}$ in the global model reflects short lifetimes of NO_x and fast-reacting NMHCs. Anthropogenic NO_x and NMHCs emitted at the surface are mostly removed from the atmosphere within the continental boundary layer [*Liang et al.*, 1998], which limits their impact on the global mean OH concentration. As seen in Table 1, increasing preindustrial CO and NMHC emissions to those of today (case B) increases S_C by 70% but decreases the global mean OH concentration by only 30%; increasing preindustrial NO_x emissions to present-day values (case C) increases S_N by a factor of 4.5 but only increases OH by 40%. The less than 10% change of the global mean OH concentration since preindustrial times in our standard model reflects the relative constancy of the $S_N/S_C^{3/2}$ ratio (Figure 5) despite factors of 4.7 and 2.5 increases in S_N and S_C, respectively.

The global increase of O_3 production in the model from preindustrial times (39 x 10^{12} mol yr^{-1}) to present (85 x 10^{12} mol yr^{-1}) reflects a combination of increasing emissions of NO_x, CO, and hydrocarbons. Although the O_3 production rate is NO_x limited throughout the troposphere [*Chameides et al.*, 1992], we find that the increase of NO_x emissions alone (case C) accounts for only 57% of the increase in O_3 production. Increases in CO and NMHC emissions (case B) and in the concentration of CH_4 (case A) make significant contributions of about 15% each, because increasing CO and hydrocarbons enhances the O_3 production efficiency per unit NO_x emitted [*Lin et al.*, 1988; *Crutzen*, 1994].

One can separate the effects of anthropogenic emissions by source category. We find that emissions from fuel combustion and industry (case D) and from biomass burning (case E) each explain about 40% of the total increase of O_3 production in the model, while the increase of CH_4 concentrations (case A) explains most of the remaining 20%. This near-additivity reflects the constancy in the O_3 yield per unit of CO or hydrocarbon emitted, as discussed below.

Fuel combustion and biomass burning make similar contributions to the rise in O_3 production even though the fossil fuel source of NO_x is larger (Table 1) because of a higher O_3 production efficiency in the tropics where most of the biomass burning source is located.

The increase of O_3 production since preindustrial times can be related quantitatively to emissions of O_3 precursors by using as diagnostic the O_3 production efficiency (α_N) per unit NO_x emitted [cf. *Liu et al.*, 1987] and the O_3 yield (α_C) per unit of CO or hydrocarbons oxidized [*Crutzen*, 1988]. The losses of CO and hydrocarbons are in balance with their sources on a global scale. The global rate of chemical O_3 production (P_{O3}) is therefore

$$P_{O3} = \alpha S \quad (1)$$

where α is α_N or α_C and S is the source of NO_x (S_N) or of CO and hydrocarbons (S_C), respectively. We obtain S_C from Table 1 by adding the sources of CO, CH_4, and NMHCs. Table 2 shows global values of α_N and α_C for all the model simulations.

We find that the O_3 production efficiency α_N has decreased by a factor of 2 since preindustrial times because of its sensitivity to NO_x concentrations [*Liu et al.*, 1987]. By contrast, the O_3 yield α_C has changed little since preindustrial times; as a result, O_3 production has increased proportionally to S_C. Increasing CO and NMHCs emissions alone (cases A and B) decreases α_C, whereas increasing NO_x emissions alone (case C) increases α_C. We find, however, that the mix of NO_x, CO, and hydrocarbon emissions from anthropogenic sources is such that it leaves α_C unchanged. The conservation of α_C explains the additivity of the forcings from fuel combustion and industry (case D), biomass burning (case E), and increasing CH_4 concentrations (case A) in increasing O_3 production since preindustrial times. Figure 6 shows a tight linear relationship between α_C and the global mean OH concentration in the model. A rise in α_C implies greater O_3 production per molecule of CO or hydrocarbon emitted and hence a net increase in OH concentrations.

We find in the model that the dependence of O_3 production on emissions of precursors is more linear when referenced to hydrocarbon rather than to NO_x emissions; that is, the variability of α_C is less than that of α_N (Table 2). As shown in the appendix, α_C is theoretically constrained to remain between 0.2 and 3; the lower limit reflects the minimum O_3 production necessary to avoid titration of OH, while the upper limit reflects the maximum O_3 yield from oxidation of a typical CO and hydrocarbon mix in a high-NO_x atmosphere [*Crutzen*, 1988].

The lower limit of α_C has two implications. Recent global three-dimensional models indicate that the budget of tropospheric O_3 is dominated by O_3 production in the troposphere, as opposed to transport from the stratosphere [*Wang et al.*, 1998b, and references therein]. This result can be simply explained by considering the lower limit of 0.2 for α_C. Our values of S_C are 120 x 10^{12} mol yr^{-1} and 48 x 10^{12} mol yr^{-1} for the present and preindustrial atmospheres, respectively (Table 1), implying minimum O_3 chemical production of 24 x 10^{12} mol yr^{-1} (present) and 10 x 10^{12} mol yr^{-1} (preindustrial). In comparison with a source of 8 x 10^{12} mol yr^{-1} transported from the stratosphere [*Wang et al.*, 1998a, b], tropospheric O_3 production must be much larger (by a factor of 3) at present and no less in preindustrial times.

Using a lower limit of 0.2 for α_C, we can also demonstrate simply that the rate of O_3 production must be NO_x limited on a global scale. Ozone production is NO_x limited if the source S_{HOx} of HO_x radicals is larger than the source S_N of NO_x; it is hydrocarbon limited if the opposite holds [*Jacob et al.*, 1995; *Kleinman et al.*, 1997]. The dominant global source of HO_x in the troposphere is O_3 photolysis to $O(^1D)$ followed by reaction of $O(^1D)$ with H_2O; this reaction is also a major sink for O_3 and amounts to 50-60% of the tropospheric O_3 source [*Crutzen*, 1994]. We thus estimate a minimum S_{HOx} of 0.2 S_C with an α_C of 0.2. In comparison, S_N=0.013 S_C for the preindustrial atmosphere, S_N=0.061 S_C for fossil fuel combustion, and S_N=0.036 S_C for biomass burning (Table 1). The dominance of S_{HOx} over S_N implies that tropospheric O_3 production has remained NO_x limited since preindustrial times and will stay so in the future as long as the global S_N/S_C ratio remains below 0.1.

6. Conclusions

We examined the changes in tropospheric O_3 and OH concentrations since preindustrial times using a global three-dimensional model. The model has been shown previously to provide a generally good simulation of O_3, CO, NO_x, and the global mean OH concentration for the present atmosphere [*Wang et al.*, 1998b]. Our simulation of the preindustrial atmosphere assumes 0.8 ppmv CH_4, no emissions from fuel combustion and industry, 10% of the present-day biomass burning source, and the same natural emissions (lightning, soils, and vegetation) as in the present.

Comparison of model results for the preindustrial atmosphere with reconstructed observations of O_3 in the nineteenth century shows significant discrepancies. The reconstructed data for O_3 over Europe and South America show concentrations of 7-12 ppbv; model results are about 5 ppbv higher and show a stronger seasonal variation. Previous global model simulations of O_3 in preindustrial times show similar overestimates. Allowing for some emissions from fossil fuel combustion in the nineteenth century would worsen the overestimates.

Of particular concern is the failure of the model to reproduce the low preindustrial O_3 observations at Pic du Midi (2.4 km altitude) which should not be affected by depositional effects or negative measurement interference by SO_2 or NH_3. A remarkable feature of the Pic du Midi observations is the lack of vertical gradient relative to sea level observations during the same period at nearby Montsouris. This lack of vertical gradient is inconsistent with our current understanding of tropospheric O_3. Matching the Pic du Midi observations in the model would require an important missing sink for O_3 in the preindustrial atmo-

sphere or a downward revision of lightning NO_x emissions (presently 3 Tg N yr^{-1}) which provide the principal source of preindustrial O_3.

Polar ice core data for preindustrial times are available for CO, CH_2O (proxy of OH), and H_2O_2 (proxy of HO_x). The model underestimates the ice core measurements of nineteenth century CO concentrations and corresponding interhemispheric gradient [*Haan et al.*, 1996]. These measurements cannot be reconciled with any reasonable CO emission inventories for the nineteenth century. Model results for OH concentrations over Greenland indicate a decrease of 12% since preindustrial times, comparable with the 30% decrease derived from ice core records of CH_2O. Model results for H_2O_2 concentrations over Greenland indicate a factor of 2.5 increase since preindustrial times; ice core records show little change of H_2O_2 concentrations until 1970 and a doubling since then.

We find that anthropogenic emissions since preindustrial times have caused an increase of 120% in tropospheric O_3 production and a doubling of the total tropospheric O_3 source (including transport from the stratosphere). The increase in the global tropospheric O_3 burden is only 63% because O_3 production due to anthropogenic emissions takes place preferentially in the lower troposphere, where the lifetime of O_3 is shorter than in the middle and upper troposphere.

Although the local rate of O_3 production in the troposphere is NO_x limited in general, we find that increasing NO_x emissions alone from preindustrial times to present explains only 57% of the rise in O_3 production of the global troposphere. Increasing emissions of CH_4, CO, and NMHCs accounts for the rest because the O_3 production efficiency per mole of NO_x emitted increases with increasing CO and hydrocarbons. Separating the effects of anthropogenic emissions by source category, we find that fossil fuel combustion and the increase of biomass burning each contribute about 40% of the global increase of O_3 production since preindustrial times in the model and that the increase of atmospheric CH_4 contributes about 20%.

The global O_3 production efficiency α_N per unit NO_x emitted decreases in the model from 60 mol/mol in preindustrial times to 28 mol/mol at present reflecting a greater relative increase of NO_x emissions (factor of 4.7) than of CO and hydrocarbons (factor of 2.5). The global O_3 yield α_C per unit CO or hydrocarbon oxidized has, however, remained nearly constant at 0.7-0.8 mol/mol; the emission mixes of NO_x, CO, and hydrocarbons from fuel combustion and industry and from biomass burning are such that they conserve α_C but not α_N. The increase of tropospheric O_3 production since preindustrial times has therefore largely followed that of CO and hydrocarbon emissions.

Model results indicate that the global mean OH concentration (weighted by air mass) has decreased by 9% since preindustrial times. However, the lifetime of CH_3CCl_3 against OH oxidation has remained at 5.1 years because of the temperature dependence of the oxidation rate constant; the increase of OH concentrations in the warmer lower troposphere has compensated for a lower global mean OH concentration. We find that the global mean OH concentration varies linearly with the $S_N/S_C^{3/2}$ ratio, where S_N and S_C are the total tropospheric sources of NO_x and of CO and hydrocarbons, respectively. The relative constancy of the global mean OH concentration since preindustrial times reflects conservation of the $S_N/S_C^{3/2}$ ratio by anthropogenic emissions.

Appendix: A Simple Schematic for Tropospheric O_3 and HO_x Chemistry

We consider here a simple schematic of tropospheric O_3-NO_x-CO chemistry derived from currently accepted mechanisms [*Logan et al.*, 1981]. The primary supply of HO_x (OH + HO_2) radical is the photolysis of O_3 to $O(^1D)$ and subsequent reaction of $O(^1D)$ with H_2O,

(R1) $O_3 + h\upsilon \rightarrow O(^1D) + O_2$

(R2) $O(^1D) + M \xrightarrow{O_2} O_3 + M$

(R3) $O(^1D) + H_2O \rightarrow 2\ OH$

Cycling of HO_x by oxidation of CO in the presence of NO_x leads to production of O_3,

(R4) $CO + OH \xrightarrow{O_2} CO_2 + HO_2$

(R5) $HO_2 + NO \rightarrow OH + NO_2$

(R6) $NO_2 + h\upsilon \xrightarrow{O_2} NO + O_3$

The oxidation of NO to NO_2 also takes place by the reaction NO + O_3,

(R7) $NO + O_3 \rightarrow NO_2 + O_2$

Loss of HO_x radicals takes place mostly by self-reaction of HO_2 and oxidation of NO_2 by OH,

(R8) $HO_2 + HO_2 \rightarrow H_2O_2 + O_2$

(R9) $OH + NO_2 \xrightarrow{M} HNO_3$

We consider in this system the steady state equations for HO_x, OH, O_3, NO_x, and CO concentrations, respectively,

$$2\frac{J_1 k_3[H_2O]}{k_2[M]}[O_3] = 2k_8[HO_2]^2 + k_9[OH][NO_2][M] \quad \text{(A1)}$$

$$k_5[HO_2][NO] + 2\frac{J_1 k_3[H_2O]}{k_2[M]}[O_3] = k_4[OH][CO] \quad \text{(A2)}$$

$$k_5[HO_2][NO] + F_{O3} = \frac{J_1 k_3[H_2O]}{k_2[M]}[O_3] + k_d[O_3] \quad \text{(A3)}$$

$$S_N = k_9\,[OH]\,[NO_2] \quad \text{(A4)}$$

$$S_C = k_4\,[OH]\,[CO] \quad \text{(A5)}$$

where k_i or J_i is the reaction or photolysis rate constant for reaction i, k_d is a deposition rate constant for O_3, F_{O3} is the net transport rate of O_3 from the stratosphere, and S_N and S_C are the sources of NO_x and CO, respectively. Hydrocarbons react similarly to CO and their sources are lumped into S_C for the purpose of this simple model. Since S_C is much larger than S_N in either the present or preindustrial atmosphere (Table 1), loss of OH radicals through reaction (R9) is negligible compared to reaction (R4) and is neglected in equation (A2).

We can now derive the chemical production rate of O_3 as that of the odd-oxygen family ($O_x \equiv O_3 + O + NO_2$) by using equations (A2), (A3), and (A5),

$$P(O_3) = k_5 [HO_2] [NO] = \frac{1}{3} (S_C - 2 (F_{O3} - k_d [O_3])) \quad (A6)$$

This chemical system is stable only if sufficient OH is available to oxidize CO. Methane observations show that the atmosphere has been stable in this manner over at least the 200,000 year extent of the ice core records [*IPCC*, 1996]. To satisfy this stability in our simple model, the production of O_3 must be at least

$$P_{O3}(\min) = \frac{1}{3} (S_C - 2 F_{O3}) \quad (A7)$$

At this limit, all O_3 molecules produced in the troposphere or transported from the stratosphere are used to generate OH radicals (R3) for the oxidation of CO (R4). In the real atmosphere, the lower limit for $P(O_3)$ is higher than that given by equation (A7) because (1) additional O_3 sinks include the reactions of O_3 with OH and HO_2, (2) additional OH sinks include the reactions of OH with O_3, H_2O_2, and H_2, and (3) additional O_3 production takes place through the reaction of NO and organic peroxy radicals in which no OH production takes place unlike in reaction (R5). Another stable chemical regime may also exist when NO_x emission is extremely low and the HO_x sources from photolysis of carbonyl compounds and the chemical recycling of peroxides become more important than the HO_x source from O_3 (reactions (R1)-(R3)). The concentrations of O_3 and OH would be extremely low under these conditions. Such a regime is not considered in this analysis.

Equation (A7) implies the existence of a lower limit for the O_3 yield α_C per unit of CO or hydrocarbons emitted,

$$\alpha_C(\min) = \frac{1}{3} (1 - 2 F_{O3} / S_C) \quad (A8)$$

Estimates of S_C and F_{O3} for preindustrial and present atmospheres (Table 1) yield a lower limit of 0.2 for α_C.

The maximum value of α_C, corresponding to high-NO_x conditions, is 1 for oxidation of CO to CO_2, 1.7 for oxidation of CH_4 to CO, and about 1 per atom C for oxidation of NMHCs to CO [*Crutzen*, 1988]. For the CO and hydrocarbon emission mixes corresponding to the preindustrial and present atmospheres, we obtain a maximum value of 3 for α_C. The total source of O_3 in the troposphere thus scales to S_C with a factor of α_C that may vary theoretically from 0.2 to 3.

The above schematic also yields a relationship between OH concentrations, S_N, and S_C. Considering equations (A1)-(A5) and assuming O_3-NO-NO_2 photochemical steady state by reactions (R6)-(R7), we obtain

$$[OH] = \frac{3^{3/2} J_1 k_3 k_5 J_6}{k_2 k_7 k_8^{1/2} k_9 [M]} \times \frac{[H_2O] \times S_N}{(S_C - 2(F_{O3} - k_d[O_3]))(S_C + F_{O3} - k_d[O_3])^{1/2}} \quad (A9)$$

Since S_C is much larger than F_{O3} in both preindustrial and present atmospheres (Table 1), this equation can be reduced to a simple dependence of [OH] on S_N and S_C

$$[OH] = K \frac{S_N}{S_C^{3/2}} \quad (A10)$$

where K is a constant. Results from our global three-dimensional model show a linear relationship between the global mean OH concentration and the $S_N/S_C^{3/2}$ ratio, but the actual dependence of [OH] on $S_N/S_C^{3/2}$ is much less than implied by the present simple box model analysis (section 5).

Acknowledgments. We thank Jennifer Logan and Clarisa Spivakovsky for helpful discussions. We also thank Bill Chameides for his comments. This work was supported by the National Aeronautics and Space Administration (EOS/IDS, ACMAP, and GTE programs).

References

Anderson, B. E., G. L. Gregory, J. D. Barrick, J. E. Collins, G. W. Sachse, M. C. Shipham, and C. H. Hudgins, Summertime tropospheric ozone distributions over central and eastern Canada, *J. Geophys. Res., 99,* 1781-1792, 1994.

Anfossi, D., and S. Sandroni, Ozone levels in Paris one century ago, *Atmos. Environ., 31,* 3481-3482, 1997.

Anfossi, D., S. Sandroni, and S. Viarengo, Tropospheric ozone in the nineteenth century: The Moncalieri series, *J. Geophys. Res., 96,* 17,349-17,352, 1991.

Anklin, M., and R. C. Bales, Recent increases in H_2O_2 concentrations at Summit, Greenland, *J. Geophys. Res., 102,* 19,099-19,104, 1997.

Berntsen, T. K., and I. S. A. Isaksen, A global three-dimensional chemical transport model for the troposphere, 1, Model description and CO and ozone results, *J. Geophys. Res., 102,* 21,239-21,280, 1997.

Berntsen, T. K., I. S. A. Isaksen, G. Myhre, J. S. Fuglestvedt, F. Stordal, T. A. Larsen, R. S. Freckleton, and K. P. Shine, Effects of anthropogenic emissions on tropospheric ozone and its radiative forcing, *J. Geophys. Res., 102,* 28,101-28,126, 1997.

Bojkov, R. D., Surface ozone during the second half of the nineteenth century, *J. Clim. Appl. Meteorol., 25,* 343-352, 1986.

Chameides, W. L., et al., Ozone precursor relationship in the ambient atmosphere, *J. Geophys. Res., 97,* 6037-6055, 1992.

Crutzen, P. J., Tropospheric ozone: A review, in *Tropospheric Ozone*, edited by I. S. A. Isaksen, pp. 3-32, D. Reidel, Norwell, Mass., 1988.

Crutzen, P. J., Global tropospheric chemistry, in *Low-Temperature Chemistry of the Atmosphere*, edited by G. K. Moortgat et al., *NATO ASI Ser., Ser. I, 21,* 465-498, 1994.

Crutzen, P. J., and P. H. Zimmermann, The changing photochemistry of the troposphere, *Tellus, 43AB,* 136-151, 1991.

Dibb, J. E., R. W. Talbot, J. W. Munger, and S.-M. Fan, Air-snow exchange of HNO_3 and NO_y at Summit, Greenland, *J. Geophys. Res., 103,* 3475-3486, 1998.

Dignon, J., and S. Hameed, Global emissions of nitrogen and sulfur oxides from 1860 to 1980, *JAPCA, 39,* 180-186, 1989.

Fuhrer, K., A. Neftel, M. Anklin, T. Staffelbach, and M. Legrand, High-resolution ammonium ice core record covering a complete glacial-interglacial cycle, *J. Geophys. Res., 101,* 4147-4164, 1996.

Ganzeveld, L., and J. Lelieveld, Dry deposition parameterization in a chemistry general circulation model and its influence on the distribution of reactive trace gases, *J. Geophys. Res., 100,* 20,999-21,012, 1995.

Haan, D., P. Martinerie, and D. Raynaud, Ice core data of atmospheric carbon monoxide over Antarctica and Greenland during the last 200 years, *Geophys. Res. Lett., 23,* 2235-2238, 1996.

Hansen, J., G. Russel, D. Rind, P. Stone, A. Lacis, S. Lebedeff, R. Ruedy, and L. Travis, Efficient three-dimensional global models for climate studies: Models I and II, *Mon. Weather Rev., 111,* 609-662, 1983.

Holton, J. R., P. H. Haynes, M. E. McIntyre, A. R. Douglass, R. B. Rood, and L. Pfister, Stratosphere-troposphere exchange, *Rev. Geophys., 33,* 403-439, 1995.

Intergovernmental Panel on Climate Change (IPCC), *Climate Change 1995, The Science of Climate Change*, edited by J. T. Houghton, et al., 572 pp., Cambridge Univ. Press, New York, 1996.

Jacob, D. J., et al., Simulation of summertime ozone over North America, *J. Geophys. Res., 98,* 14,797-14,816, 1993.

Jacob, D. J., L. W. Horowitz, J. W. Munger, B. G. Heikes, R. R. Dickerson, R. S. Artz, and W. C. Keene, Seasonal transition from NO_x- to hydrocarbon-limited ozone production over the eastern United States in September, *J. Geophys. Res., 100,* 9315-9324, 1995.

Kasibhatla, P., H. Levy II., A. Klonecki, and W. L. Chameides, Three-dimensional view of the large-scale tropospheric ozone distribution over the North Atlantic Ocean during summer, *J. Geophys. Res., 101,* 29,305-29,316, 1996.

Kirchhoff, V. W. J. H., and R. A. Rasmussen, Time variations of CO and O_3 concentrations in a region subject to biomass burning, *J. Geophys. Res., 95,* 7521-7532, 1990.

Kleinman, L. I., P. H. Daum, J. H. Lee, Y. N. Lee, L. J. Nunnermacker, S. R. Springston, L. Newman, J. Weinsteinlloyd, and S. Sillman, Dependence of ozone production on NO and hydrocarbons in the troposphere, *Geophys. Res. Lett., 24,* 2299-2302, 1997.

Lelieveld, J., and R. Van Dorland, Ozone chemistry changes in the troposphere and consequent radiative forcing of climate, in *Atmospheric Ozone as a Climate Gas*, edited by W.C. Wang and I. S. A. Isaksen, pp. 227-258, Springer-Verlag, New York, 1995.

Levy, H., II, P. S. Kasibhatla, W. J. Moxim, A. A. Klonecki, A. I. Hirsch, S. J. Oltmans, and W. L. Chamedies, The global impact of human activity on tropospheric ozone, *Geophys. Res. Lett., 24,* 791-794, 1997.

Liang, J., L. W. Horowitz, D. J. Jacob, Y. Wang, A. M. Fiore, J. A. Logan, G. M. Gardner, and J. W. Munger, Seasonal variation of photochemistry over North America and its implications for the export of ozone and reactive nitrogen to the global atmosphere, *J. Geophys. Res., 103,* 13,435-13,450, 1998.

Lin, X., M. Trainer, and S. C. Liu, On the nonlinearity of the tropospheric ozone production, *J. Geophys. Res., 98,* 15,879-15,888, 1988.

Linvill, D. E., W. J. Hooker, and B. Olson, Ozone in Michigan's environment 1876-1880, *Mon. Weather Rev., 108,* 1883-1891, 1980.

Lissac, I., and V. Grubisich, An analysis of surface ozone data measured at the end of the 19th century in Zagreb, Yugoslavia, *Atmos. Environ., Part A, 25,* 481-486, 1991.

Liu, S. C., M. Trainer, F. C. Fehsenfeld, D. D. Parrish, E. J. Williams, D. W. Fahey, G. Hubler, and P. C. Murphy, Ozone production in the rural troposphere and the implications for regional and global ozone distributions, *J. Geophys. Res., 92,* 10,463-10,482, 1987.

Logan, J. A., M. J. Prather, S. C. Wofsy, and M. B. McElroy, Tropospheric chemistry: A global perspective, *J. Geophys. Res., 86,* 7210-7254, 1981.

Marenco, A., H. Gouget, P. Nedelec, and J.-P. Pages, Evidence of a long-term increase in tropospheric ozone from Pic du Midi data series, Consequences: Positive radiative forcing, *J. Geophys. Res., 99,* 16,617-16,632, 1994.

Martinerie, P., G. P. Brasseur, and C. Granier, The chemical composition of ancient atmosphere: A model study constrained by ice core data, *J. Geophys. Res., 100,* 14,291-14,304, 1995.

Mauzerall, D. L., D. J. Jacob, S.-M. Fan, J. D. Bradshaw, G. L. Gregory, G. W. Sachse, and D. R. Blake, Origin of tropospheric ozone at remote high northern latitudes in summer, *J. Geophys. Res., 101,* 4175-4188, 1996.

Mayewski, P. A., and M. R. Legrand, Recent increase in nitrate concentration of Antarctic snow, *Nature, 346,* 258-260, 1990.

Mayewski, P. A., W. B. Lyons, M. J. Spencer, M. S. Twickler, C. G. Buck, and S. Whitlow, An ice-core record of atmospheric response to anthropogenic sulphate and nitrate, *Nature, 346,* 554-556, 1990.

Munger, J. W., S. M. Fan, P. S. Bakwin, M. L. Goulden, A. H. Goldstein, A. S. Colman, and S. C. Wofsy, Regional budgets for nitrogen oxides from continental sources: Variations of rates for oxidation and deposition with season and distance from source regions, *J. Geophys. Res., 103,* 8355-8368, 1998.

Neftel, A., R. C. Bales, and D. J. Jacob, H_2O_2 and HCHO in polar snow and their relation to atmospheric chemistry, in *Ice Core Studies of Global Biogeochemical Cycles*, edited by R. Delmas, *NATO ASI Ser., Ser. I, 30,* 249-264, 1995.

Prinn, R. G., R. F. Weiss, B. R. Miller, J. Huang, F. N. Alyea, D. M. Cunnold, P. J. Fraser, D. E. Hartley, and P. G. Simmonds, Atmospheric trends and lifetime of CH_3CCl_3 and global OH concentrations, *Science, 269,* 187-192, 1995.

Roelofs, G.-J., J. Lelieveld, and R. Van Dorland, A three-dimensional chemistry/general circulation model simulation of

anthropogenically derived ozone in the troposphere and its radiative climate forcing, *J. Geophys. Res., 102*, 23,389-23,401, 1997.

Sandroni, S., D. Anfossi, and S. Viarenzo, Surface ozone levels at the end of nineteenth century in South America, *J. Geophys. Res., 97*, 2535-2539, 1992.

Sigg, A., and A. Neftel, Evidence for a 50% increase in H_2O_2 over the past 200 years from a Greenland ice core, *Nature, 351*, 557-559, 1991.

Staffelbach, T., A. Neftel, B. Stauffer, and D. J. Jacob, Formaldehyde in polar ice cores: a possibility to characterize the atmospheric sink of methane in the past?, *Nature, 349*, 603-605, 1991.

Thompson, A. M., The oxidizing capacity of the Earth's atmosphere: Probable past and future changes, *Science, 256*, 1157-1168, 1992.

Thompson, A M., J. A. Chappellaz, I. Y. Fung, and T. L. Kucsera, The atmospheric CH_4 increase since the last glacial maximum, *Tellus, Ser. B, 45*, 242-257, 1993.

Volz, A., and D. Kley, Evaluation of the Montsouris series of ozone measurements made in the nineteenth century, *Nature, 332*, 240-242, 1988.

Wang, Y., D. J. Jacob, and J. A. Logan, Global simulation of tropospheric O_3-NO_x-hydrocarbon chemistry, 1, Model formulation, *J. Geophys. Res., 103*, 10,713-10,726, 1998a.

Wang, Y., J. A. Logan, and D. J. Jacob, Global simulation of tropospheric O_3-NO_x-hydrocarbon chemistry, 2, Model evaluation and global ozone budget, *J. Geophys. Res., 103*, 10,727-10,756, 1998b.

Wang, Y., D. J. Jacob, and J. A. Logan, Global simulation of tropospheric O_3-NO_x-hydrocarbon chemistry, 3, Origin of tropospheric ozone and effects of non-methane hydrocarbons, *J. Geophys. Res., 103*, 10,757-10,768, 1998c.

Zander, R., P. Demoulin, D. H. Ehhalt, U. Schmidt, and C. P. Rinsland, Secular increase of the total vertical column abundance of carbon monoxide above central Europe since 1950, *J. Geophys. Res., 94*, 11,021-11,028, 1989.

Table 1. Global Sources of NO_x, CO and Hydrocarbons, and Global Mean OH Concentrations

		Sensitivity Simulations Departing from the Preindustrial Atmosphere[b]					
	Preindustrial[a]	A 1.7 ppmv CH_4	B Present CO + NMHCs	C Present NO_x	D Present Fuel + Industry	E Present Biomass Burning	Present[c]
NO_x (S_N)	0.64	0.64	0.64	2.9	2.1	1.4	3.0
CO and Hydrocarbons							
CO[d]	24	34	58	29	45	43	76
CH_4[e]	14	24	10	20	15	15	29
Nonmethane hydrocarbons (NMHCs)	10	10	13	10	12	11	13
Total (S_C)	48	68	81	59	72	69	118
Global mean OH[f]	1.15	0.95	0.78	1.56	1.18	1.19	1.04

Sources of NO_x and of CO and hydrocarbons are in Tmol yr^{-1}; global mean OH concentrations are in 10^6 molecules cm^{-3}.

[a]Preindustrial emissions include NO_x from lightning, unfertilized soils, and 10% of present-day biomass burning, isoprene and acetone from terrestrial vegetation, and CO and NMHCs from 10% of present-day biomass burning. Methane concentration is specified at 0.8 ppmv.

[b]The sensitivity cases include A, preindustrial atmosphere with present-day CH_4 concentration of 1.7 ppmv; B, preindustrial atmosphere with present-day emissions of CO and NMHCs from fuel combustion, industry, and biomass burning; C, preindustrial atmosphere with present-day NO_x emissions from fossil fuel combustion and biomass burning (but not including soil emissions from fertilizer use of 0.1 Tmol yr^{-1}); D, preindustrial atmosphere with present-day NO_x, CO and NMHC emissions from fuel combustion and industry; E, preindustrial atmosphere with present-day biomass burning emissions of NO_x, CO, and NMHCs.

[c]*Wang et al.* [1998a].

[d]Including direct CO emission and CO production from hydrocarbon oxidation.

[e]Source needed to sustain the specified concentration of CH_4 (0.8 ppmv in the preindustrial simulation and sensitivity simulations B-E, 1.7 ppmv in sensitivity simulation A and the present-day simulation).

[f]Weighted by atmospheric mass in the column up to 150 mbar.

Table 2. Global Sources, Sinks, and Production Efficiencies for Tropospheric O_3

		Sensitivity Simulations Departing from the Preindustrial Atmosphere					
	Preindustrial	A 1.7 ppmv CH_4	B Present CO + NMHCs	C Present NO_x	D Present Fuel + Industry	E Present Biomass Burning	Present
Sources (Tmol yr^{-1})							
Chemical production	39	46	45	65	59	55	85
Transport from stratosphere	8.4	8.4	8.4	8.4	8.4	8.4	8.4
Sinks (Tmol yr^{-1})							
Chemical loss	38	44	44	60	54	52	77
Dry deposition	8.7	9.8	9.6	13	13	11	17
O_3 burden (Tmol)	4.0	4.5	4.4	5.2	5.1	4.7	6.5
O_3 lifetime (days)	31	31	31	26	28	27	25
O_3 production efficiency α_N per of NO_x emitted (mol/mol)	60	71	70	22	28	39	28
O_3 yield α_C per unit of CO or hydrocarbon oxidized (mol/mol)	0.80	0.67	0.56	1.1	0.81	0.80	0.72

The budgets and production efficiencies are for odd oxygen ($O_x = O_3 + O + NO_2 + HNO_4 + 2 \times NO_3 + 3 \times N_2O_5$ + organic nitrates + HNO_3) in the model air column from the surface to 150 mbar (specified as the tropopause). Over 95% of O_x is O_3. Chemical production of O_x is by reactions of peroxy radicals with NO, and chemical loss is principally through the reactions O^1D+H_2O, O_3+HO_2, and O_3+OH. Sensitivity cases are the same as in Table 1.

Figure Captions (Double Column)

Figure 1. Simulated July mean concentrations (ppbv) of O_3 and CO in the lowest model layer (0-500 m above surface) for the preindustrial and present atmospheres.

Figure 2a. Zonally averaged annual mean concentrations of O_3 (ppbv), OH (10^5 molecules cm^{-3}), NO_x (pptv), and CO (ppbv) as a function of pressure and latitude for the preindustrial and present atmospheres.

Figure 2b. Percentage changes of O_3, OH, NO_x, and CO concentrations (shown in Figure 2a) from preindustrial times to present.

Figure 3. Simulations and reconstructed observations of preindustrial O_3 concentrations (ppbv) in surface air over Europe and South America: Montsouris, France (1876-1886) [*Anfossi et al.*, 1991], Pic du Midi, France (1874-1881, the Plantade Station, Elevation 2.4 km) [*Marenco et al.*, 1994], Moncalieri, Italy (1868-1893) [*Anfossi et al.*, 1991], Cordoba, Argentina (1886-1892) [*Sandroni et al.*, 1992], and Montevideo, Uruguay (1883-1885) [*Sandroni et al.*, 1992]. Reconstructed observations are open circles; results from the standard preindustrial simulation (with biomass burning source reduced to 10% of the present-day value) are solid lines; results from a preindustrial simulation without the O_3 source from the stratosphere are dotted lines; and results from a preindustrial simulation with the present-day biomass burning source (NO_x, CO, and NMHCs) are dashed lines.

Figure 4. Measured and simulated preindustrial CO concentrations (ppbv) over Greenland and Antarctica. Ice core measurements by *Haan et al.* [1996] (annual averages) represented in solid lines are for the periods of 1802-1862 (Greenland) and 1860-1916 (Antarctica). Dotted lines are results from the standard preindustrial simulation with the biomass burning source reduced to 10% of the present-day value, and dashed lines are results from a preindustrial simulation with the present-day biomass burning source (NO_x, CO, and NMHCs).

Figure 5. Global mean OH concentration as a function of $S_N/S_C^{3/2}$, where S_N and S_C are the tropospheric sources of NO_x and of CO and hydrocarbons (mol yr^{-1}), respectively. The solid line shows a least squares fit. Model sensitivity simulations are described in Table 1.

Figure 6. The O_3 yield α_C (mol/mol) per unit CO or hydrocarbon oxidized as a function of the global mean OH concentration (10^6 molecules cm^{-3}). The solid line shows a least squares fit. Model sensitivity simulations are described in Table 1.

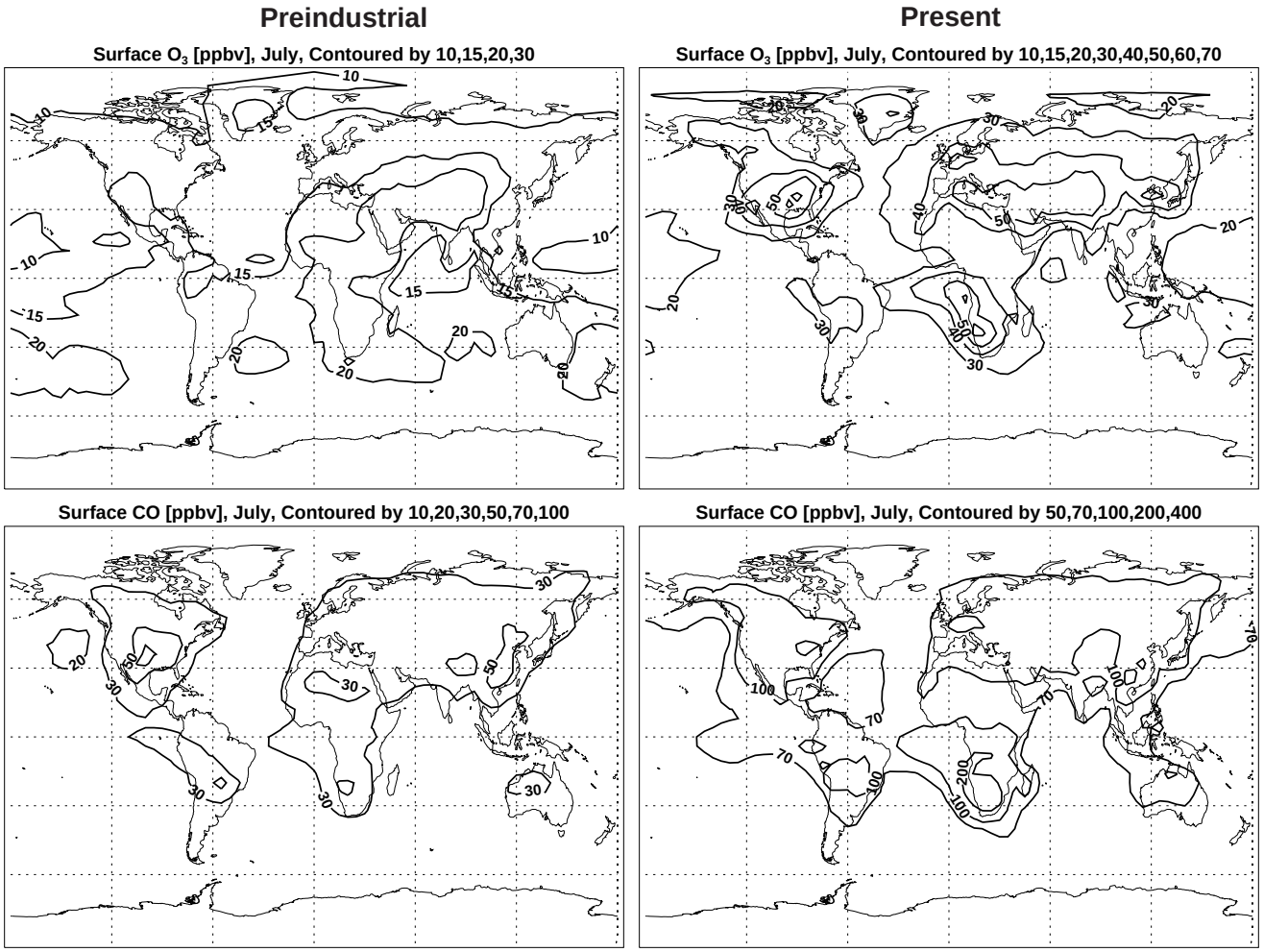
Preindustrial
Present
Surface O_3 [ppbv], July, Contoured by 10,15,20,30
Surface O_3 [ppbv], July, Contoured by 10,15,20,30,40,50,60,70
Surface CO [ppbv], July, Contoured by 10,20,30,50,70,100
Surface CO [ppbv], July, Contoured by 50,70,100,200,400

Fig. 1 (Bottom)

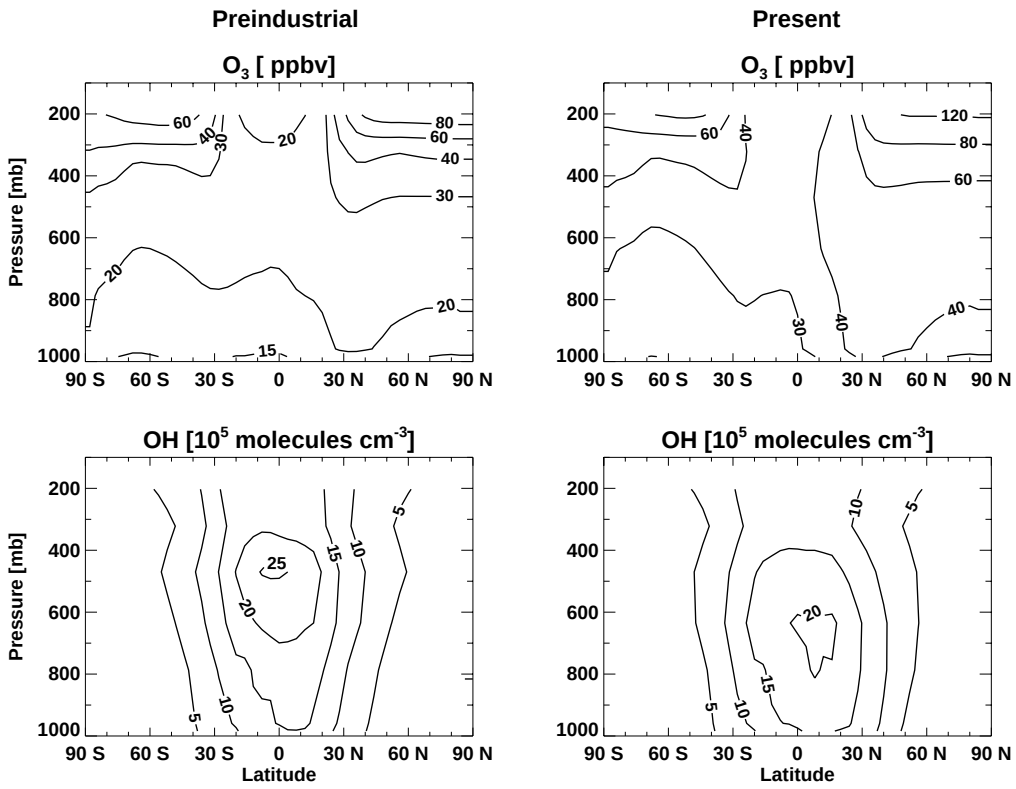

Fig. 2a. Part I (Bottom)

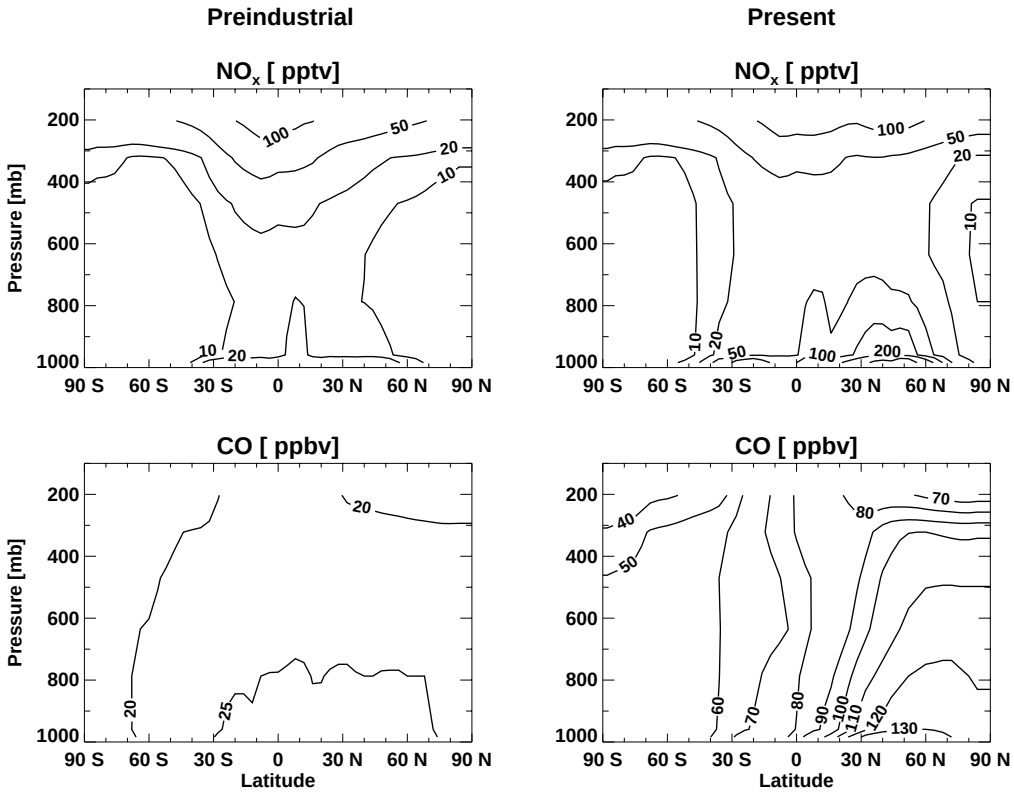

Fig. 2a. Part II (Bottom)

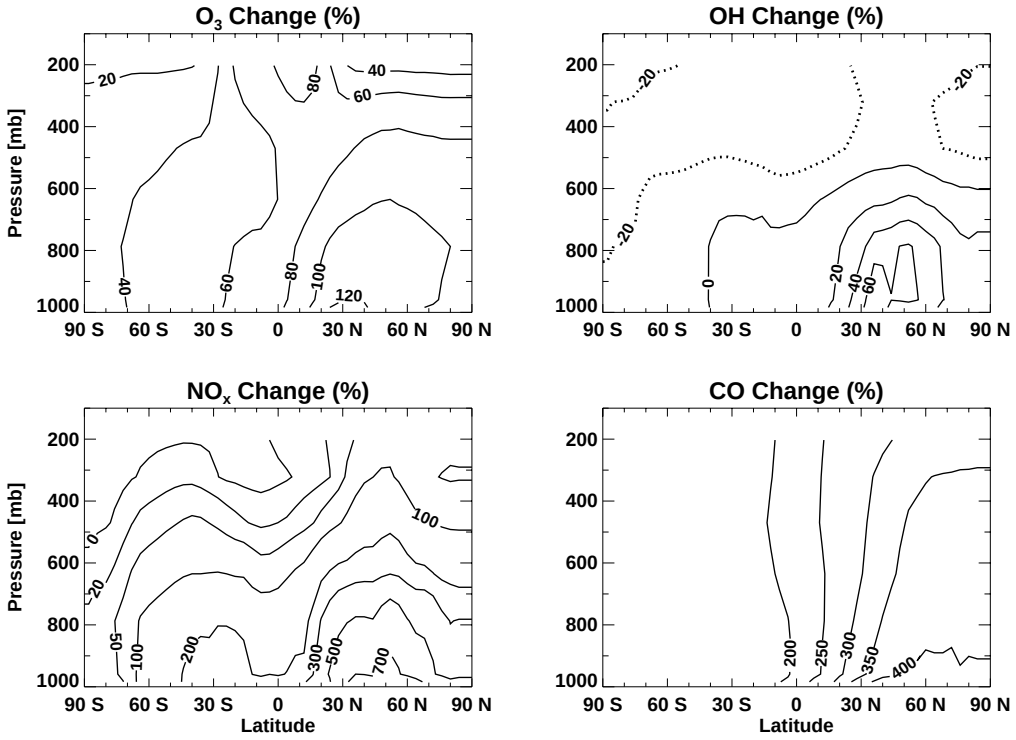

Fig. 2b (Bottom)

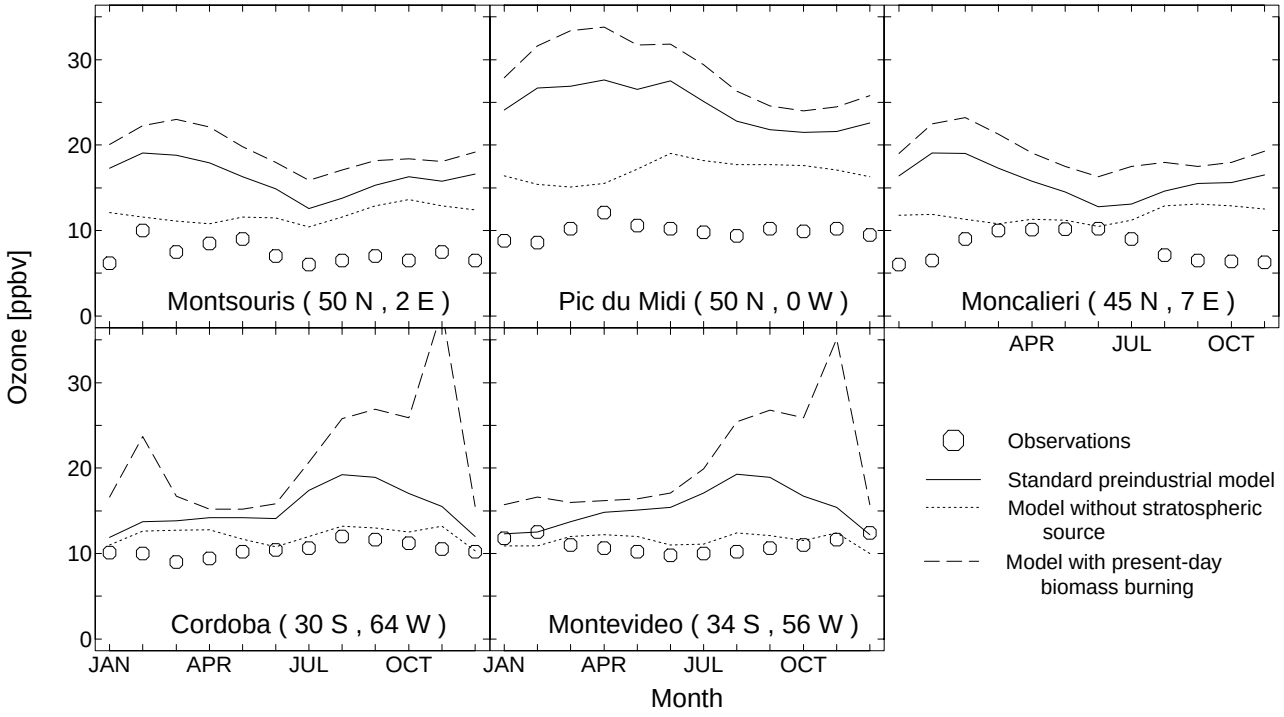
Ozone [ppbv]
30
20
10
0
Montsouris (50 N , 2 E)
Pic du Midi (50 N , 0 W)
Moncalieri (45 N , 7 E)
APR
JUL
OCT
Cordoba (30 S , 64 W)
Montevideo (34 S , 56 W)
JAN
APR
JUL
OCT
Month
Observations
Standard preindustrial model
Model without stratospheric source
Model with present-day biomass burning

Fig. 3 (Bottom)

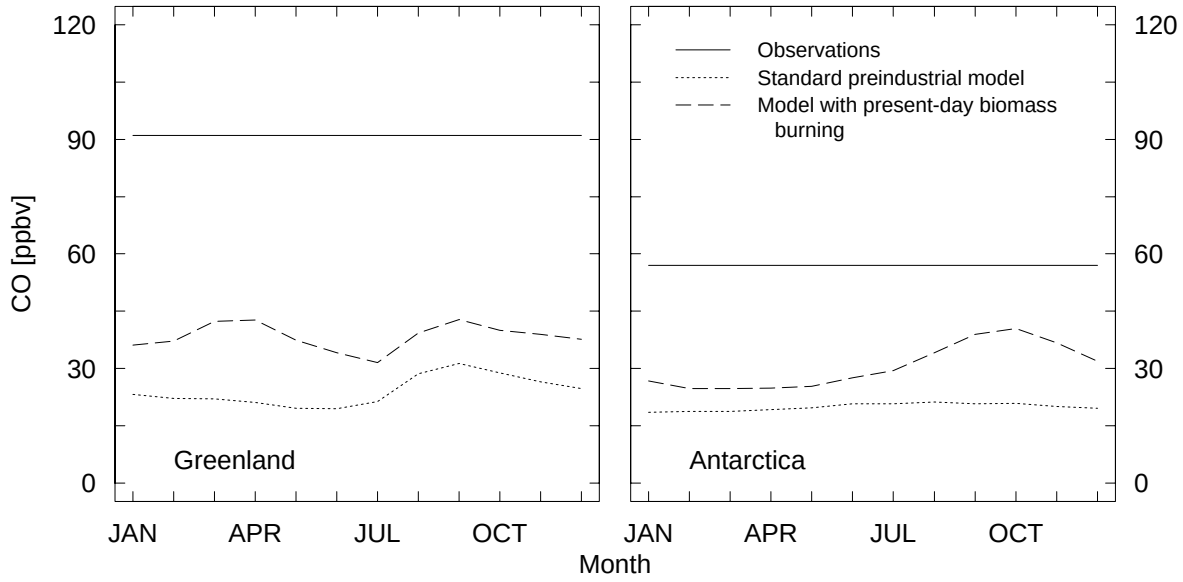
120
90
60
30
0
CO [ppbv]
Observations
Standard preindustrial model
Model with present-day biomass burning
Greenland
Antarctica
JAN
APR
JUL
OCT
Month

Fig. 4 (Bottom)

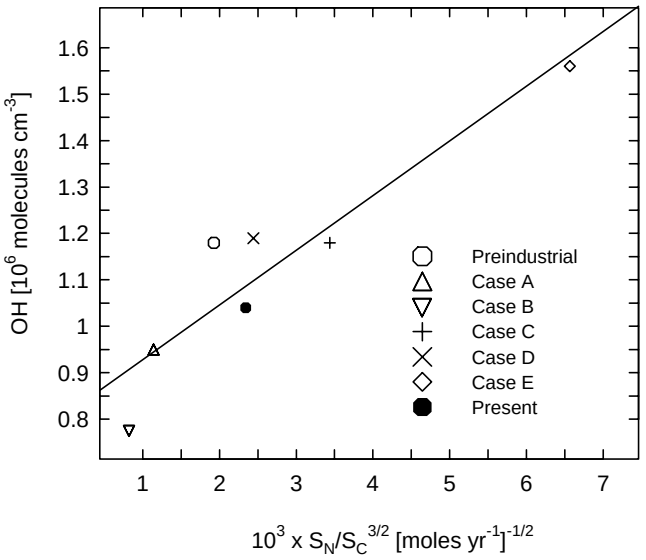
1.6
1.5
1.4
1.3
1.2
1.1
1
0.9
0.8
OH [10^6 molecules cm^-3]
1
2
3
4
5
6
7
10^3 x S_N/S_C^3/2 [moles yr^-1]^-1/2
Preindustrial
Case A
Case B
Case C
Case D
Case E
Present

Fig. 5 (Bottom)

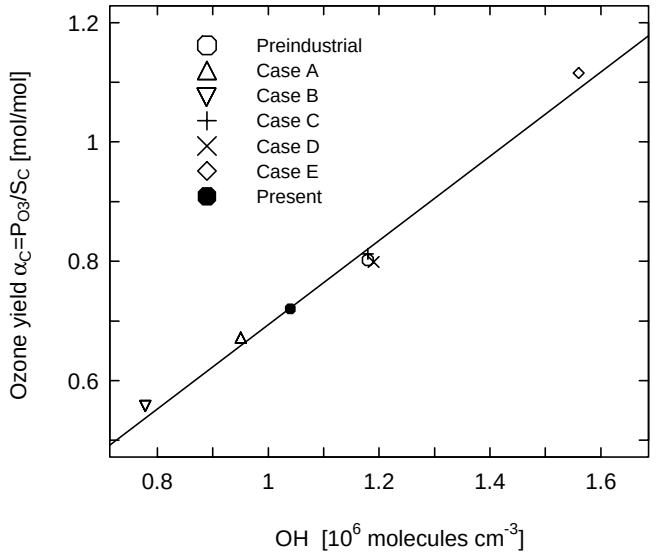
Preindustrial
Case A
Case B
Case C
Case D
Case E
Present
Ozone yield $\alpha_C=P_{O3}/S_C$ [mol/mol]
OH [10^6 molecules cm^{-3}]
1.2
1
0.8
0.6
0.8
1
1.2
1.4
1.6

Fig. 6 (Bottom)